Biochimica et Biophysica Acta 1848 (2015) 593–602

Contents lists available at ScienceDirect

Biochimica et Biophysica Acta

journal homepage: www.elsevier.com/locate/bbamem

The role of tryptophans on the cellular uptake and membrane interaction of arginine-rich cell penetrating peptides

Marie-Lise Jobin [a], Marine Blanchet [a], Sarah Henry [a], Stéphane Chaignepain [a], Claude Manigand [a], Sabine Castano [a], Sophie Lecomte [a], Fabienne Burlina [b], Sandrine Sagan [b], Isabel D. Alves [a,*]

[a] CBMN-Univ Bordeaux, UMR 5248, Allée Geoffroy St Hilaire, 33600 Pessac, France
[b] Sorbonne Universités — UPMC Univ Paris 06, École Normale Supérieure-PSL Research University, Département de Chimie, CNRS UMR 7203 LBM, 4 Place Jussieu, F-75005 Paris, France

ARTICLE INFO

Article history:
Received 26 July 2014
Received in revised form 10 November 2014
Accepted 12 November 2014
Available online 20 November 2014

Keywords:
Cell penetrating peptide
Peptide/lipid interaction
Lipid model systems

ABSTRACT

Cell-penetrating peptides (CPP) are able to efficiently transport cargos across cell membranes without being cytotoxic to cells, thus present a great potential in drug delivery and diagnosis. While the role of cationic residues in CPPs has been well studied, that of Trp is still not clear. Herein 7 peptide analogs of RW9 (RRWWRRWRR, an efficient CPP) were synthesized in which Trp were systematically replaced by Phe residues. Quantification of cellular uptake reveals that substitution of Trp by Phe strongly reduces the internalization of all peptides despite the fact that they strongly accumulate in the cell membrane. Cellular internalization and biophysical studies show that not only the number of Trp residues but also their positioning in the helix and the size of the hydrophobic face they form are important for their internalization efficacy, the highest uptake occurring for the analog with 3 Trp residues. Using CD and ATR-FTIR spectroscopy we observe that all peptides became structured in contact with lipids, mainly in α-helix. Intrinsic tryptophan fluorescence studies indicate that all peptides partition in the membrane in about the same manner (Kp ~ 10^5) and that they are located just below the lipid headgroups (~10 Å) with slightly different insertion depths for the different analogs. Plasmon Waveguide Resonance studies reveal a direct correlation between the number of Trp residues and the reversibility of the interaction following membrane washing. Thus a more interfacial location of the CPP renders the interaction with the membrane more adjustable and transitory enhancing its internalization ability.

1. Introduction

One of the major obstacles to the use of large therapeutic molecules or imaging agents having intracellular targets is their low permeability through biomembranes. One of the breakthroughs of the last 20 years is the discovery of cell-penetrating peptides (CPP) as molecules capable of internalizing into cells in a receptor- and energy-independent way and without being toxic to cells. Their great potential relies on the fact that they can transport a great variety of cargoes into cells both in terms of size and nature and some CPPs are even already used as drug delivery vector (for a review, see [1]). Green & Loewenstein and Frankel & Pabo discovered the first CPP almost simultaneously in 1988 [2,3]. They found that the Tat protein from HIV-1 was internalized into cells and Vives et al., found in 1997 the minimal sequence that was responsible for the protein internalization [4]. Following this finding, penetratin was discovered in 1994 by the group of Alain Prochiantz [5]. This is a peptide derived from the homeodomain of the Drosophila homeobox *Antennapedia* and was shown to possess a good internalization efficacy. Since then a large number of Structure/Activity Relationship studies have been performed both to study their membrane-translocating capabilities and to design novel sequences with greater efficacy and better selectivity. Since the Tat peptide possesses a large number of basic residues (6 Arg and 2 Lys on 13 residues) Wender and Rothbard discovered that a polyarginine comporting 9 residues is an efficient CPP [6]. Futaki's group then synthesized oligoarginines of different lengths (R_n with $6 < n < 12$) and studied their internalization efficiency [7]. They could determine that 8 Arg residues were sufficient to confer the polyarginine cell penetrating properties. Different derivatives of penetratin have also been synthetized and it was observed that the internalization was based neither on the chirality of the peptide, nor its amphiphilicity or its secondary structure [5,8]. Regarding the mechanisms implicated in their cellular internalization, it has been generally accepted that both endocytosis and direct translocation through the membrane are implicated in their uptake. The balance

Abbreviations: AMP, Anti-microbial Peptide; ATR-FTIR, Attenuated Total Reflectance-Fourier Transform Infrared; CPP, cell-penetrating peptide; CD, Circular dichroism; CHO, Chinese hamster ovary; DOPC, Dioleoylphosphatidylcholine; DOPG, Dioleoylphosphatidylglycerol; DLS, Dynamic light scattering; GAG, Glycosaminoglycan; HSPG, Heparan sulfate proteoglycans; LUV, Large unilamellar vesicle; MALDI, Matrix-Assisted Laser Desorption/Ionization; MLV, Multi lamellar vesicle; MS, Mass spectrometry; PC, Phosphatidylcholine; PG, Phosphatidylglycerol; PWR, Plasmon Waveguide Resonance; SAR, Structure/Activity Relationship; SUV, Small Unilamellar Vesicles

* Corresponding author. Tel.: +33 5 40 00 68 49.
E-mail address: i.alves@cbmn.u-bordeaux.fr (I.D. Alves).

http://dx.doi.org/10.1016/j.bbamem.2014.11.013
0005-2736/

between the two mechanisms depends on a great variety of aspects such as the nature and size of the CPP and its cargo, the nature of the link between the two, the temperature at which internalization experiments are conducted, the cell lines used, among other parameters [9–12]. Electrostatic interactions between the positive charges in the peptide and negative charges in the cell membrane surface have been shown to be essential during the first stage of interaction with the membrane. The presence of basic amino acids in the sequence has been well studied and Arg residues have been reported to be especially important for cellular internalization. It was shown that the uptake efficiency is attributed to the type of bond formed between Arg and the lipid headgroups rather than the charges presented to the membrane. Indeed Arg can form bidentate hydrogen bonds that interact simultaneously with phosphate moieties on multiple lipid headgroups while Lys residues can only form monodentate hydrogen bonds that interact with the phosphate moiety on a single headgroup [13,14]. Guanidinium-rich peptides also establish strong electrostatic interactions with negatively charged heparan sulfate proteoglycans (HSPG) on the cell surface, important as a first recognition and their accumulation in the membrane [15,16]. The presence of hydrophobic residues for internalization has also been investigated. The substitution of the Trp^{48} and Trp^{56} by Phe abolished totally the internalization of penetratin [17]. From these studies, the Arg-rich CPP RW9 (RRWWRRWRR) was designed and determined to possess very high cellular uptake efficiency [18]. Biological studies on RW9 have revealed an important decrease in internalization in GAG-deficient cells evidencing that proteoglycans at the membrane surface are important for its cellular internalization [19]. Biophysical studies have shown its preferential interaction with anionic model membranes corroborating biological studies on the importance of electrostatic interactions between peptide and membranes. Previous studies on RL9 (RRLLRRLRR), an analog of RW9 where Trp residues were replaced by Leu residues have shown that this peptide was not internalized into cells despite the fact that it accumulated in the membrane [19,20]. At the same time, oligoarginine peptide (R_9) possessing no aromatic residues internalizes very well in eukaryotic cells at approximately the same level as RW9 [19]. The main question addressed here is to understand the role of the Trp in membrane translocation regarding the RW9 sequence. Therefore, we synthesized 7 peptides in which Phe systematically replaced Trp residues (RX9) (Table 1). The strategy was to keep the hydrophobicity but specially the aromaticity of the hydrophobic residues, because previous NMR studies on RW9 evidenced the existence of π–cation interactions between certain Arg and Trp residues [19].

Quantification of the total amount of internalized peptides (all intracellular compartments included) shows that the replacement of all Trp residues almost completely abolished the peptide internalization while the substitution of 1 or 2 Trp strongly decreases their internalization efficiency. To understand these differences in cellular internalization we have decided to investigate the interaction of these peptides with lipid membranes and therefore shed some light into their membrane crossing and translocation. It should be noted that direct translocation through the cell membrane is just one of the many mechanisms used by CPPs to internalize, nonetheless a good understanding of CPP interaction with lipids is important. For that we have used lipid model systems and different biophysical approaches in an attempt to correlate their cellular uptake and membrane direct translocation with bilayer interaction. Since electrostatic interactions were found to be important for the membrane interaction of Arg-rich peptides with cellular membranes [see [21] for a review] we have included anionic lipids in the model membranes used. Even though anionic lipids are very weakly present in eukaryotic cell membrane, especially in the outer leaflet, the few anionic lipids present (~2%) can have their potential enhanced by assembling into domains, a property reported to be induced by certain CPPs [22]. Although, the outer leaflet of healthy eukaryotic membranes possesses almost no anionic lipids, important electrostatic interactions between the CPPs and GAG can be established. Often biophysicists have employed anionic lipids just to mimic the overall anionic character of the cell membrane surface, which is also our approach here. Additionally it should be noted that during certain cellular dysfunctions such as when cells become tumoral or enter apoptosis, the amount of anionic lipids in their outer leaflet (mostly phosphatidylserine) increases up to 9%, rendering the cellular membrane significantly more anionic [23–26]. CD and ATR-FTIR were used to investigate the secondary structure of the peptides in contact with model membranes to define if there was a correlation between their tendency to adopt a secondary structure in the presence of lipids and their internalization capacities. No direct correlation was found. Their cytotoxicity on cells and effect on model membranes were explored. The replacement of Trp by Phe induced no cytotoxicity or dye leakage although the peptides bind and slightly perturb the membrane. The affinity and insertion depth of the peptides were studied by Plasmon Waveguide Resonance and Trp fluorescence and a correlation with their internalization capacities was established.

Table 1
Amino-acid sequences of the RX9 peptides used in this study.

	Peptide sequence	MW (Da)	Charges (at pH 7)
RW9	Biotin(O_2)-GGGG-RRWWRRWRR-NH_2	1999	6
RFFF9	Biotin(O_2)-GGGG-RRFFRRFRR-NH_2	1882	6
RFFW9	Biotin(O_2)-GGGG-RRFFRRWRR-NH_2	1921	6
RWFF9	Biotin(O_2)-GGGG-RRWFRRFRR-NH_2	1921	6
RFWF9	Biotin(O_2)-GGGG-RRFWRRFRR-NH_2	1921	6
RFWW9	Biotin(O_2)-GGGG-RRFWRRWRR-NH_2	1960	6
RWWF9	Biotin(O_2)-GGGG-RRWWRRFRR-NH_2	1960	6
RWFW9	Biotin(O_2)-GGGG-RRWFRRWRR-NH_2	1960	6

2. Materials & methods

2.1. Materials

All lipids were obtained from Avanti Polar Lipids (Alabaster, AL, USA). The calcein and acrylamide were obtained from Sigma Aldrich. Biotin(O_2)-($[^1H]$-G)$_4$-RRFFRRFRR-NH_2(RF_9), Biotin(O_2)-($[^1H]$-G)$_4$-RRFFRRWRR-NH_2($RFFW_9$), Biotin(O_2)-($[^1H]$-G)$_4$-RRWFRRFRR-NH_2($RWFF_9$), Biotin(O_2)-($[^1H]$-G)$_4$-RRFWRRFRR-NH_2 ($RFWF_9$), Biotin(O_2)-($[^1H]$-G)$_4$-RRFWRRWRR-NH_2 ($RFWW_9$), Biotin(O_2)-($[^1H]$-G)$_4$-RRWWRRFRR-NH_2($RWWF_9$), Biotin(O_2)-($[^1H]$-G)$_{44}$-RRWFRRWRR-NH_2($RWFW_9$) and Biotin(O_2)-($[^2H]$-G)$_4$-RRFFRRFRR-NH_2, Biotin(O_2)-($[^2H]$-G)$_4$-RRFFRRWRR-NH_2, Biotin(O_2)-($[^2H]$-G)$_4$-RRWFRRFRR-NH_2, Biotin(O_2)-($[^2H]$-G)$_4$-RRFWRRFRR-NH_2, Biotin(O_2)-($[^2H]$-G)$_4$-RRFWRRWRR-NH_2, Biotin(O_2)-($[^2H]$-G)$_4$-RRWWRRFRR-NH_2, Biotin(O_2)-($[^2H]$-G)$_4$-RRWFRRWRR-NH_2 were synthesized using the Fmoc solid-phase strategy ($[^1H]$-G and $[^2H]$-G correspond to non-deuterated and bi-deuterated glycine, respectively). The oxidation protocol of the biotin was as follows: 10 g of biotin was dissolved in 40 mL of H_2O_2 (30% in H_2O) and 120 mL of AcOH was added. The mixture was stirred at room temperature for few hours and a precipitate was formed. The precipitate was filtered, washed with Et_2O and dried under vacuum. Oxidation efficiency of the biotin was checked by liquid-state NMR. Biotin sulfone was coupled to the peptide under the same conditions used for the amino-acid coupling. Peptides were purified by High Performance Liquid Chromatography (HPLC), in a reverse phase column (RP) C18 using H_2O/CH_3CN/TFA gradient. MALDI-TOF mass spectrometry was used to characterize the peptides. To efficiently remove the TFA counter-ion a simple method was used that consists in lyophilizing the sample 3 times in the presence of 10 mM HCl directly replacing TFA counter-ions with chloride ions [27]. A low concentration of HCl was used to prevent peptide degradation. The removal of TFA was followed by ^{19}F-NMR.

2.2. Cell culture

Wild type Chinese hamster ovary CHO-K1 (WT) cells were cultured in Dulbecco's modified Eagle's medium (DMEM) supplemented with

10% fetal calf serum (FCS), penicillin (100,000 IU/L), streptomycin (100,000 IU/L), and amphotericin B (1 mg/L) in a humidified atmosphere containing 5% CO_2 at 37 °C.

2.3. Cell viability assays

Cell viability was measured using the Dojindo Cell-Counting Kit 8 based on the reduction of a reagent into a colored product by viable cell dehydrogenases. CHO-K1 cells were seeded in a 96-well plate 1 day before treatment (4000 cells per well). Cells were treated with 5 μM, 10 μM, 20 μM or 50 μM peptide for 1 h, 6 h and 24 h. Untreated cells were defined as living cell control (negative control) and 0.3% Triton X-100 as maximum cytotoxicity (positive control).

2.4. Cellular uptake and quantification of membrane-bound peptide

Cellular uptake was quantified using the method described by Burlina et al. [28]. In this protocol, the studied peptides bear a tag composed of four glycine residues together with a biotin moiety for purification purposes. After 1 h incubation of 10 μM peptide and washing, a protease is added (0.05% Pronase in Tris–HCl buffer, 100 mM pH 7.5) in order to detach the cells and to degrade all the non-internalized or membrane-bound peptides. This avoids overestimating the quantity of internalized peptide due to the presence of peptides attached to the outer leaflet of the membrane. The cells are then lysed (0.3% Triton, 1 M NaCl) and boiled and the cell lysate is incubated with streptavidin-coated magnetic beads to extract the peptide from the lysate. This protocol gives access to the total amount of intact internalized peptide. For quantification of total cell-associated CPP (non-washable membrane-bound + internalized peptide), the same experimental conditions were used except that no protease was added and the cells were directly lysed. The peptides are eluted from the streptavidin-coated magnetic beads with HCCA matrix and spotted on the MALDI plate. Mass spectrometry is not a quantitative method per se, therefore an internal standard is added to the lysis solution. This standard peptide has the same sequence as the one to quantify except that it bears a tag composed of four bi-deuterated glycine residues instead of four glycine residues. This allows the quantification of internalized and membrane-bound peptide. The samples were analyzed by MALDI-TOF MS (positive ion reflector mode) on a Voyager DEPRO mass spectrometer (Applied Biosystems).

2.5. Preparation of liposomes

All liposomes were prepared by initially dissolving the appropriate amount of phospholipids, to obtain the desired concentration, in chloroform and methanol to ensure the complete mixing of the components. A lipid film was then formed by removing the solvent using a stream of N_2 (g) followed by 3 h under vacuum. To form MLVs the dried lipids were dispersed in buffer (either 10 mM Tris, 150 mM NaCl, 2 mM EDTA or 10 mM phosphate buffer depending on the technique used) and thorough vortexed. To form LUVs the MLV dispersion was run through five freeze/thawing cycles and passed through a mini-extruder equipped with two stacked 0.1 μm polycarbonate filters (Avanti, Alabaster, AL). SUVs were prepared by tip sonication after direct hydration of the lipid film.

2.6. Dynamic light scattering experiments

The experiments were performed using the Zetasizer Nano (Malvern) system with an ALV Laser goniometer, which consisted of a 35 mW HeNe linear polarized laser with a wavelength of 632.8 nm and an ALV-5000/EPP Multiple Tau Digital correlator with 125 ns initial sampling time. The measurements were carried out at 173°. All measurements were performed at room temperature (25 °C) in phosphate buffer. To get an insight into the influence of the peptides on LUV integrity, 40 μL of a 1 mg/mL LUV solution was analyzed by DLS, followed by the addition of a small volume of peptide (1 mM) to the LUV suspension to the desired P/L ratio (1/100, 1/50, 1/25, 1/10) and particle size again analyzed, immediately.

2.7. Circular dichroism experiments

CD data were recorded on a Jasco J-815 CD spectrophotometer with a 1 mm path length. Far-UV spectra were recorded from 180 to 270 nm with a 0.5 nm step resolution and a 2 nm bandwidth at 37 °C. The scan speed was 50 nm/min (0.5 s response time), and the spectra were averaged over 8 scans. CD spectra were collected for all the peptides in phosphate buffer with and without liposomes at different P/L ratios (1/50, 1/25, 1/10). For each sample, the background (buffer) was automatically subtracted from the signal. Spectra were smoothed using a Savitzky–Golay smoothing filter. Spectra were deconvoluted using the software CDFriend previously developed in our laboratory (S. Buchoux, not published).

2.8. ATR-FTIR spectroscopy

Small Unilamellar Vesicles (SUV) composed of DOPC or DOPC:DOPG (4:1) were prepared in a solution of D_2O. SUVs were burst on a germanium ATR crystal to form a single bilayer which is controlled by the measurement of the absolute IR intensity. ATR spectra were recorded on a Nicolet 6700 spectrometer ThermoScientific equipped with a MCT detector cooled at 77 K. Since ATR spectroscopy is sensitive to the orientation of the structures, spectra were recorded with parallel (p) and perpendicular (s) polarizations of the incident light with respect to the ATR plate [29,30]. 400 scans were recorded at a resolution of 4 cm^{-1}. All the orientation information are then contained in the dichroïc ratio $R_{ATR} = Ap/As$, where Ai represents the absorbance of the considered band at p or s polarization of the incident light.

The resulting spectra were analyzed with an algorithm based on a second-derivative function and a self-deconvolution procedure (GRAMS and OMNIC softwares, ThermoFisher Scientific) to determine the number and wavenumber of individual bands within the spectral range 1600–1690 cm^{-1}. The amide I band of each spectrum could be fitted by four bands assigned to the vibration of amide I involved in four different secondary structures (Fig. S2). Vibrational assignments of the infrared band components in the amide I region were made according to Goormaghtigh et al. [29,30]. The fit was obtained with a mixed Lorentzian (25%)–Gaussian (75%) band profile and width at half-height included between 20% and 25%. The relative contributions of the different bands were determined from the fit results obtained for the amide I band. The amount of each secondary-structure element is given as a percentage (Table 2) and is determined by dividing the integral intensity of one amide I band component by the total intensity of all amide I band components. The standard error does not exceed 1.5%. For all spectra, fit results correspond to a local minimum at the end of the iteration procedure.

Table 2
Viability assays (in percentage) for the RX9 peptides for a peptide concentration of 5 μM and with different incubation times. The experiments have been performed twice and each time in triplicate.

	1 h	6 h	24 h
RFFF9	104 ± 13	65 ± 10	105 ± 2
RFFW9	104 ± 25	66 ± 10	90 ± 5
RWFF9	91 ± 28	62 ± 9	78 ± 8
RFWF9	103 ± 23	57 ± 9	78 ± 5
RFWW9	85 ± 14	51 ± 8	76 ± 4
RWWF9	80 ± 20	51 ± 8	76 ± 20
RWFW9	75 ± 6	54 ± 8	77 ± 9

2.9. Calcein leakage experiments

Calcein-containing LUVs were made using the same protocol used to make regular LUVs, except for the hydration step of the lipid films that was made with Tris buffer containing 70 mM calcein. The protocol to prepare calcein-loaded vesicles was the same as previously described by Jobin et al. [31]. For the assay, the lipid concentration was set at 1 μM and peptide concentration was allowed to vary from 10 nM to 100 nM (P/L ratio of 1/100 to 1/10 respectively). All measurements were performed on 96-well microplates using a Perkin Elmer LS55 spectrometer (Buckinghamshire, UK). Data were collected every minute at room temperature using a λ_{exc} at 485 nm and λ_{em} at 515 nm with an emission and excitation slit of 2.5 nm.

The fluorescence intensity at the equilibrium was measured after 1.5 h. At the end of the assay, complete leakage of LUVs was achieved by adding 10 μL of 10% Triton X-100 solution dissolving the lipid membrane without interfering with the fluorescence signal. The percentage of calcein release was calculated according to the following equation:

$$\%\ \text{calcein leakage} = \frac{Ft - F0}{Ff - F0} * 100 \quad (1)$$

where the percent of calcein leakage is the fraction of dye released (normalized membrane leakage), Ft is the measured fluorescence intensity at time t, and F0 and Ff are respectively the fluorescence intensities at times t = 0, and after final addition of Triton X-100, respectively. A dilution correction was applied on the fluorescence intensity after injection of the Triton X-100. Each experiment was repeated three times.

2.10. Fluorescence spectroscopy measurements

2.10.1. Nernst partition coefficient experiments

Peptide–phospholipid interactions were studied by monitoring the changes in the Trp fluorescence emission spectra of the peptides upon addition of LUVs. Intrinsic Trp fluorescence of the peptides was measured before and after addition of different amounts of phospholipid vesicles to a 0.5 μM peptide solution. Trp fluorescence was measured at room temperature on a Spex Fluoromax-4 (Horiba) spectrofluorometer.

Emission spectra were recorded between 300 and 500 nm with an excitation wavelength of 280 nm, slit widths of 5 nm for excitation and 10 nm for emission. Peptide–lipid binding was determined from the quenching of the intrinsic Trp fluorescence intensity of the peptides upon addition of LUVs. The maximum fluorescence intensity was plotted vs. the added lipid concentration and fitted using the simple partition model (2), the self-quenching model (3) and the three-state partition model well described by Melo & Castanho [32]. The data were analyzed using Origin.

$$\frac{I}{I_w} = \frac{1 + K_p \gamma_L [L] I_L / I_w}{1 + K_p \gamma_L [L]} \quad (2)$$

$$\frac{I}{I_w} = \frac{1 + K_p \gamma_L [L] I_L / I_w}{1 + K_p \gamma_L [L] + k_2 K_p I_L} + \frac{1}{1 + K_p \gamma_L [L]} \quad (3)$$

where [L] is the total phospholipid concentration available for the peptide to interact with, K_p is the Nernst partition constant, k_2 is proportional to the ratio between the bimolecular self-quenching rate and the radiative decay rate, γ_L is the phospholipids molar volume, which is 0.763 M^{-1} for the lipid used in this study. I_L and I_W are the fluorescence intensities the mixture would display if all the peptide was in the lipidic or aqueous phase, respectively. I_W can be obtained from the measurement of I in the absence of lipid; I_L is a limit value of fluorescence intensity as [L] → ∞ and is determined as a system parameter together with K_p.

2.10.2. Brominated lipid quenching experiments

Depth-dependent fluorescence quenching of tryptophan was performed in LUVs composed of DOPC, DOPC:DOPG 4:1, and either (6,7)-, (9,10)-, or (11,12)-BrPC at molar ratios of 70:30 with DOPC:BrPC and 50:20:30 with DOPC:DOPG:BrPC. Fluorescence intensities in the absence of quencher (F0) were measured in DOPC and DOPC:DOPG (4:1) vesicles. Spectra were recorded between 300 and 500 nm with an increment of 1 nm and an integration time of 0.1 s, using an excitation wavelength of 280 nm. The P/L molar ratio was 1:50 and the peptide concentration was 0.5 μM (for RW9, RWFF9, RFWF9 and RWWF9) and 0.8 μM (for $RFWW_9$). Data were corrected for vesicle background, and the total intensity was calculated as the sum of all measured points in each spectrum. Depth-dependent fluorescence quenching profiles (DFQPs) were fitted to data in Matlab using the Distribution Analysis (DA) method [33,34] as well as the parallax method (PM) [35–38].

$$\text{DA}: \ln \frac{F_0}{F_{(h)}} = \frac{S}{\sigma\sqrt{2\pi}} \exp\left[-\frac{(h - h_m)^2}{2\sigma^2}\right] \quad (4)$$

$$\text{PM}: \ln \frac{F_0}{F_{(h)}} = \pi C\left[R_c^2 - (h - h_m)^2\right] \quad (5)$$

In the equations above, F_0 is the fluorescence intensity in the absence of quencher, $F_{(h)}$ is the intensity in the presence of quencher at the distance h (Å) from the bilayer center, and h_m is the average insertion depth of the tryptophan residues. In DA the DFQP data are fitted with a Gaussian function where σ denotes the dispersion, which is related to the in-depth distribution of the tryptophan chromophores, and S is the area under the quenching profile, which is related to the quenchability of the tryptophan moiety. The Parallax Method fits data to a truncated parabola, and R_c is the radius of quenching. Average bromine distances from the bilayer center (h) were taken to be 11.0, 8.3, and 6.5 Å for (6,7)-BrPC, (9,10)-BrPCand (11,12)-BrPC, respectively [38].

2.10.3. Acrylamide quenching experiments

Peptide–lipid interactions are accompanied by changes in the accessibility of the peptides to aqueous quenchers of Trp fluorescence. Acrylamide quenching experiments were carried out on a 0.5 μM peptide solution in the absence or presence of LUVs by addition of aliquots of 4 M acrylamide solution. The peptide/lipid mixtures (P/L molar ratio of 1/50) were incubated for 15 min at room temperature prior to the measurements. The excitation wavelength was set to 295 nm instead of 280 nm to reduce absorbance by acrylamide. Fluorescence intensities were measured after addition of quencher at room temperature. The quenching constants were obtained from the slope of the Stern–Volmer plots of F_0/F vs. [quencher], with F_0 and F as the fluorescence intensities in the absence and presence of quencher, respectively. The normalized accessibility factor (naf) was calculated in comparison with the K_{sv} for each peptide in buffer.

2.11. Plasmon Waveguide Resonance measurements

Experiments were performed on a beta PWR instrument from Proterion Corp. (Piscataway, NJ) that had a spectral angular resolution of 1 mdeg. The technique used to form supported bilayers was the same that the one previously described by Salamon et al. [39–41]. Data were fitted (GraphPad Prism) through a hyperbolic saturation curve providing the dissociation constants. It should be noted that since concomitantly with the binding process other processes, such as membrane reorganization and solvation occur, the dissociation constants correspond to apparent dissociation constants. In order to test for binding reversibility following peptide binding at saturating concentrations, the PWR cell sample was washed twice, by flowing

buffer through the cell. Following that the spectra were acquired for both polarizations. A comparison of the resonance angles before and after washing gives information about the reversibility in the P/L interaction.

3. Results & discussion

3.1. Effect of the peptides on the cell viability

The cell viability was tested with all RX9 peptides and was first studied to investigate whether the replacement of Trp residues changes their cytotoxicity (Table 2). The cell viability was measured on CHO-K1 cells using the CCK8 test providing the rate of viable cells. Concentrations varied between 5 and 50 μM and peptides were incubated for 1, 6 and 24 h at 37 °C. None of the peptides has shown any significant cytotoxicity at these concentrations at 1 h (which corresponds to the incubation time used to quantify cellular uptake). However we noticed a decrease of the cell viability for longer incubation time (6 h and 24 h). This demonstrates that the replacement of Trp by Phe residues in the sequence affects the cytotoxicity of the peptides.

3.2. Quantification of cellular uptake and membrane-bound peptide

Quantification of cellular uptake of each peptide was investigated by a protocol already published that uses MALDI-TOF mass spectrometry as the analytical technique [28]. The experiments were performed with CHO-K1 cells at 37 °C, a temperature at which both endosomal and cytosolic peptides were quantified and at which peptides can enter through both endocytosis and direct translocation [42,43]. The results show that all RX9 peptides are much less internalized (~1 pmol or less) than RW9 (~10 pmol), about a ten-fold decrease (Fig. 1A). The least internalized peptide (only ~0.2 pmol) is observed for the analog containing no Trp residues (RF9). The analogs containing 1 or 2 Trp residues are slightly more internalized (~1 pmol) than RF9 but show no difference between them. The results indicate that the presence of Trp residues in RW9 analogs is important for their cellular internalization. Since the first contact between the peptide and the cell is through the cell membrane, quantification of membrane-bound peptide was performed. Overall, the results show that RX9 peptides accumulate in the membrane in the same extent as RW9 (~250 pmol) (Fig. 1B). Membrane accumulation at 4 °C provides similar results (data not shown). In terms of the two extreme behaviors, the peptide RWFF9 accumulates the most in the membrane (~450 pmol), while the peptide RFWW9 accumulates the least (~100 pmol). These results show that the presence of Trp residues is important for RX9 cellular internalization. No correlation exists between the amount of membrane-bound and that of internalized peptide in the RX9 series.

From the cellular uptake results we have selected for further studies 5 peptides that appeared to be the most representative of the RX9 series, notably with variable number of Trp residues and significant differences in internalization capacities. We have therefore chosen the peptide without Trp residues (RF9), 2 peptides containing 1 Trp (RFWF9 and RWFF9) and 2 peptides with 2 Trp (RFWW9 and RWWF9). Biophysics experiments aimed at characterizing their interaction with lipid membranes in an attempt to correlate that with the differences in terms of cellular uptake efficacy were performed on the 5 selected peptides (described in the next sections).

3.3. Peptide secondary structure

As with RW9, the CD spectra of the RX9 peptides were strongly affected by the π–π stacking occurring between aromatic residues [19]. In the case of RF9, RFWW9 and RWWF9 (3 Phe and 1 respectively), a negative band around 230 nm was also observed that prevented proper spectral decomposition (Fig. S1). This band is negative in the case of the RWWF9 and positive in the case of the RFWF9 as it depends on the

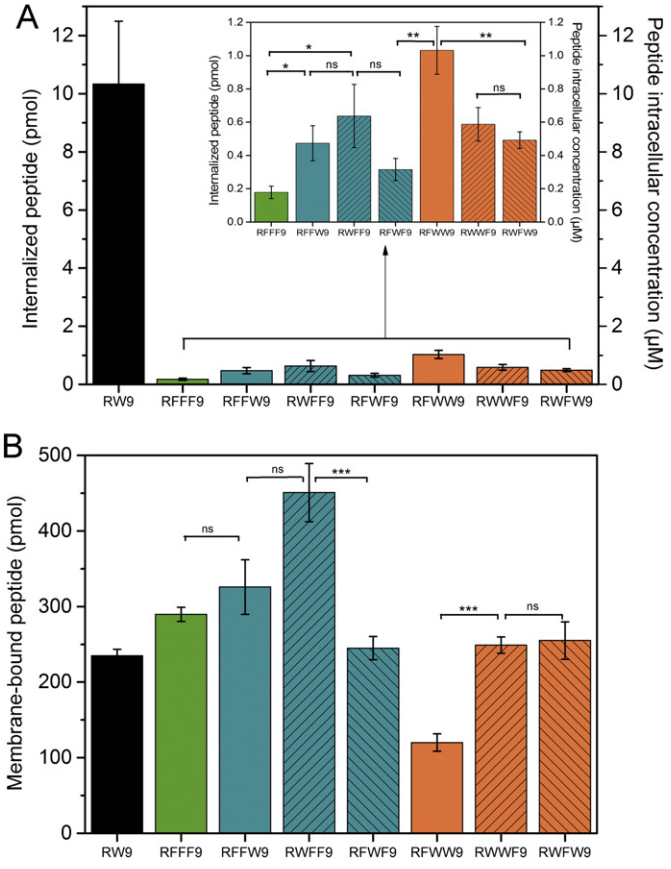

Fig. 1. (A) MALDI-TOF MS quantification of RX9 and RW9 internalization in 1 million CHO-K1 cells after peptide incubation for 1 h at 37 °C. (B) Membrane-bound peptide quantification on CHO-K1 cells (1 million) determined by mass spectrometry (MALDI-TOF) at 37 °C. Significance was tested using a Student t test: ns: $p > 0.05$; *$0.01 < p < 0.05$; **$0.01 < p < 0.001$; ***$p < 0.005$.

orientation of the aromatic residues. Peptides with 2 Phe (RFWF9 and RWFF9) gave more interpretable results as no absorbance was observed at 230 nm allowing data decomposition and secondary structure determination. In buffer and in the presence of zwitterionic lipids, the peptides are in random coil conformation with a small α-helix contribution (~10%; Fig. S1). In the presence of anionic lipids, 2 negative bands at 208 and 222 nm are observed indicating α-helix structuration (~20%; Fig. S1). Helical structuration in the presence of anionic liposomes was also observed in the case of RW9 [19]. Moreover a preferential π–cation interaction between residues Arg^8 and Trp^4 and Trp^7 was evidenced by solution NMR by Walrant et al. [19]. Since we replaced Trp^4 and Trp^7 by Phe in some cases, those interactions might have been affected. Indeed, the most internalized peptide for the RX9 series is RFWW9, which retains Trp^4 and Trp^7 and thus preserves these interactions. Therefore π–cation interactions seem to affect peptide internalization. This is to be expected since such interactions partially mask the charge of the peptide allowing a less energetically unfavorable membrane crossing.

The results indicate that the replacement of some Trp by Phe residues does not change the secondary structure of RX9 in interaction with lipids and so the secondary structure upon lipid contact is not directly correlated to the internalization. The possibility of a correlation between the capacity of a CPP to adopt a particular secondary structure and to translocate is so far not clear in the literature. For example in the case of penetratin it has been shown that α-helical structure is not necessary for its internalization [8,44].

The secondary structure of the peptides in contact with lipids was also investigated by ATR-FTIR spectroscopy to avoid this issue caused by the aromatic residues (Table 3). We have found that the secondary

Table 3
RX9 peptide secondary structure percent determined by ATR-FTIR spectroscopy.
*RC: random coil.

	Buffer				DOPC				DOPC:DOPG			
Peptides	RC*	α-Helix	β-Sheet	β-Turn	RC*	α-Helix	β-Sheet	β-Turn	RC*	α-Helix	β-Sheet	β-Turn
RFFF9	19	35	32	14	24	37	11	28	20	41	27	12
RWFF9	29	41	11	19	28	46	12	14	30	28	31	11
RFWF9	22	33	19	26	19	34	20	27	32	33	28	7
RFWW9	52	26	7	15	23	38	27	12	29	37	26	8
RWWF9	30	31	22	17	25	38	22	15	31	40	18	11

structures of RX9 peptides were not well defined corresponding mostly to a mixture of peptides adopting different secondary structures. Thus we were unable to perform spectral decomposition and determine with certainty the type and amount of each secondary structure. However we observed a marked increase in helical content in the presence of membranes, especially those containing anionic lipids.

3.4. Peptide effect on membrane supramolecular organization and integrity

Dynamic light scattering (DLS) experiments were performed in order to investigate the influence of the peptides on liposome size and distribution. Measurements were acquired in the absence and presence of peptide and at different P/L ratios. Table S1 presents the variation in size distribution of liposomes composed of DOPC, DOPG and DOPC:DOPG (4:1 mol:mol) and for a P/L ratio of 1/50. In the case of DOPC the size of the liposomes was not significantly modified by peptide addition but the size of anionic liposomes (DOPG and DOPC:DOPG) increased importantly (up to 100 nm size increase) in the presence of the peptides. This shows that aggregation or fusion of anionic liposomes is induced by peptide addition. The same observation was reported by Walrant et al. on the effect of RW9 on anionic lipids by following changes in turbidity [19]. No significant differences among the RX9 analogs were observed indicating that lipid interactions are mostly driven by electrostatic forces and therefore by the number of Arg residues which is the same for all peptides.

Calcein leakage experiments were performed to investigate whether RX9 peptides perturbed liposome membrane integrity (e.g. pore formation). In the case of anionic liposomes almost no leakage was observed (less than 1%) following 1 h peptide incubation at a P/L ratio of 1/50, meaning that the membrane integrity was not affected by the addition of the RX9 peptides. In the case of zwitterionic liposomes the leakage was slightly higher (below 5%) indicating that RX9 peptides slightly perturbed these liposomes (Table S2). We have observed that the leakage was similar (<5%) for all peptides and at all P/L ratios (1/100 to 1/10; data not shown) so we assumed that this could result from a saturation of the bilayer surface by the peptide that induced a slight leakage. Overall, the results indicate that the peptides do not significantly perturb the membrane integrity (no pore formation), which are in agreement with cell viability results.

Table 4
Partition coefficients (K_p) of the RX9 peptides with increasing concentration of liposomes (from 2.5 μM to 200 μM) at constant peptide concentration (0.5 μM). The experiments have been done in duplicate at room temperature.

	Kp (.10^5)		
	DOPC	DOPC/DOPG (4:1)	DOPG
RW9	2.0 ± 0.8	3.8 ± 0.2	1.5 ± 0.6
RWFF9	4.6 ± 0.5	3.1 ± 0.5	1.6 ± 0.2
RFWF9	2.15 ± 0.05	1.765 ± 0.005	1.88 ± 0.07
RFWW9	3.4 ± 0.7	1.77 ± 0.06	2.51 ± 0.07
RWWF9	3.0 ± 0.5	0.9 ± 0.6	1.4 ± 0.2

3.5. Peptide interaction and partitioning with model membranes

The intrinsic Trp fluorescence of the peptides was used to characterize the partitioning of the RX9 peptides with model membranes. The Nernst partition coefficient (K_p) was calculated at a constant peptide concentration from the fluorescence intensity (I) vs. lipid concentration ([L]) plots using the titration method already described [45,46]. The coefficient K_p is the ratio between membrane-bound and aqueous phase peptide concentrations. For all lipid systems the K_p obtained was in the range of 10^5 evidencing the importance of electrostatic recognition in P/L interaction [47] (Table 4). This is consistent with the fact that RX9 peptides are positively charged at physiological pH (6+) (Table 1) and thus can establish important electrostatic interactions

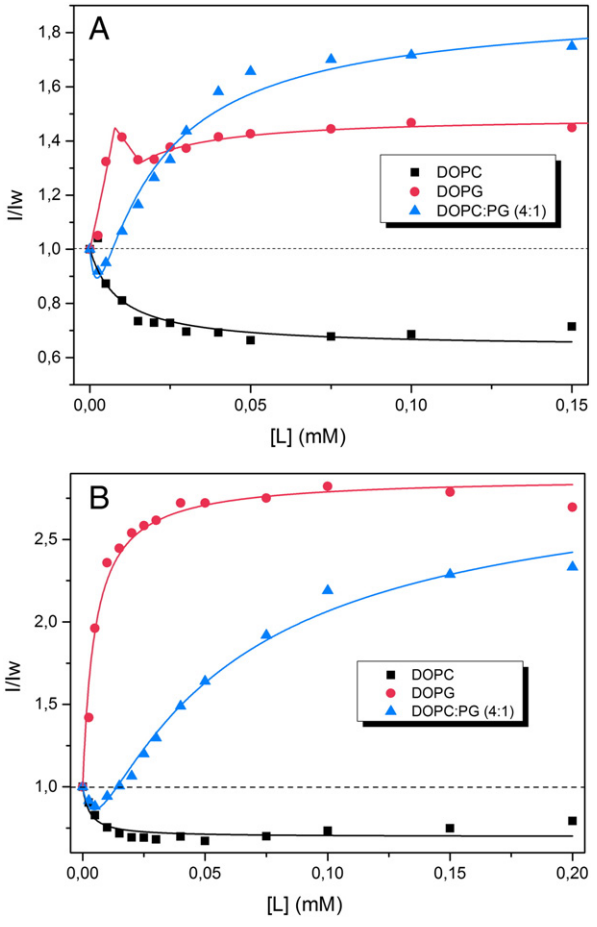

Fig. 2. Partition curves of RW9 (A) and RFWW9 (B) peptides in the presence of liposomes. The peptide concentration used was 0.5 μM and the lipid stock concentration was 0.1 mM and 1 mM. The data were fitted with Eq. (2) for DOPC and DOPG curves in the case of RFWF9, RFWW9 and $RWWF_9$, Eq. (3) was used to fit the DOPC:DOPG (4:1 mol:mol) curves and the three-state model equations were used to fit DOPG curves of RW9 and RWFF9.

with the negative phosphate groups in the lipid headgroups. Overall the partition of the different peptides was comparable independently of the lipid composition.

Even though the K_p among the RX9 and RW9 peptides was the same, partition curves were different depending on liposome composition. In the case of DOPC fluorescence intensity of the peptides decreased upon lipid contact with a hyperbolic behavior but with no shift in the maximum wavelength fluorescence (Fig. 2).

This results from dynamic quenching of the Trp fluorescence following the interaction of the peptides with the lipid polar headgroups. The absence of shift in the maximum wavelength fluorescence upon lipid contact suggests that the peptide might be adsorbed to the membrane with the same hydrophilic environment as when in solution and therefore it is not deeply inserted in the hydrophobic core.

This behavior was slightly different in the presence of liposomes containing DOPG (DOPC:DOPG 4:1). The same decrease in fluorescence intensity was observed at low lipid concentrations and then at a higher lipid concentration a hyperbolic increase appeared along with a blue shift of ~10 nm in the maximum fluorescence intensity (Fig. 2). This behavior has already been reported and results from peptide self-quenching upon bilayer insertion [32,48]. The Trp inserts more deeply in the bilayer at the lipid acyl chain region changing its environment to a more hydrophobic one. This different behavior in terms of Trp fluorescence in the presence of anionic lipids in the membrane was confirmed with experiments on pure DOPG liposomes where a three-step process was observed (Fig. 2A). In the first phase, at low lipid concentrations, the maximum fluorescence intensity increases but no blue shift appears indicating that the peptide interacts with the membrane without inserting deeply in the hydrophobic core. This first superficial contact might be the consequence of strong electrostatic interactions between the Arg and the negative charges of DOPG. In the second phase, at higher lipid concentrations, a large blue shift is observed (~20 nm) with a small decrease in intensity for certain peptides (RW9 and RWFF9) followed by an increase until a plateau is reached (Fig. 2A). For the peptides RFWF9, RFWW9 and RWWF9, the curve profile is only hyperbolic. This increase in fluorescence maximum is due to solvent effects, which increase Trp quantum yield that is also evidenced by the blue-shift. This corroborates with a deep insertion of the peptide into the bilayer with the Trp residues oriented toward the hydrophobic core of the membrane. These two-stage membrane interaction and insertion were already proposed by Walrant et al. for RW9, demonstrating that Arg residues act as an hinge by means of, in an initial stage, electrostatic interactions with the anionic lipids and then a deeper Trp insertion in a second stage [49].

The K_p observed was similar among the RX9 peptides and more surprisingly for the different lipid systems. This indicates that the proportion of membrane-bound peptide, relative to the free one, is the same whatever the membrane composition but the kinetics and affinity of interaction might be different (this is further described below). The number and position of Trp does not seem to affect the partitioning of the peptides in the membrane indicating that electrostatic interactions play a major role in this process.

Based on the blue shift observed with anionic liposomes we could determine a "half-binding" corresponding to the concentration of lipids necessary to reach 50% of the blue-shift (Fig. S2). The half-binding was much lower with DOPG than with DOPC:DOPG LUVs. This confirms that peptide interaction with the membrane is enhanced in the presence of anionic lipids. To further investigate the insertion of the peptides into liposomes of different compositions, we have calculated the Stern–Volmer constant (K_{SV}) by doing acrylamide-quenching experiments (Fig. 3). We have normalized the results to the K_{SV} in the buffer to obtain the normalized accessibility factor (naf). This allows us to compare the results obtained among the different peptides. The results show that Trp residues of all peptides upon contact with zwitterionic liposomes are almost totally exposed to the buffer (60 to 90% of accessibility). They are more buried in the presence of partially anionic liposomes

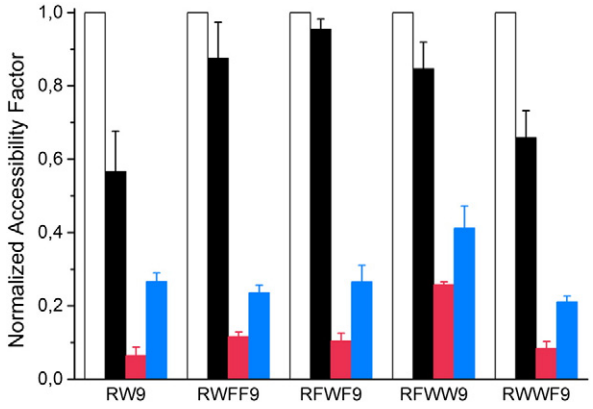

Fig. 3. Normalized accessibility factor (naf) of the RX9 peptides determined from the Stern–Volmer constants normalized relatively to the K_{SV} in buffer. The bars represent the naf for buffer (white), DOPC (black), DOPG (red) and DOPC:DOPG (4:1 mol:mol) (blue) liposomes. Experiments were done in triplicate at room temperature.

(20 to 30 % of accessibility) and almost completely with pure DOPG liposomes (10 to 20% of accessibility). No significant differences were observed among the RX9 and RW9 peptides with this technique.

Plasmon Waveguide Resonance (PWR) was used to study the affinity of the RX9 for zwitterionic and anionic lipids and the effect in the membrane organization. Upon peptide addition a decrease in the resonance angle was observed for both *p*- and *s*-polarization indicating

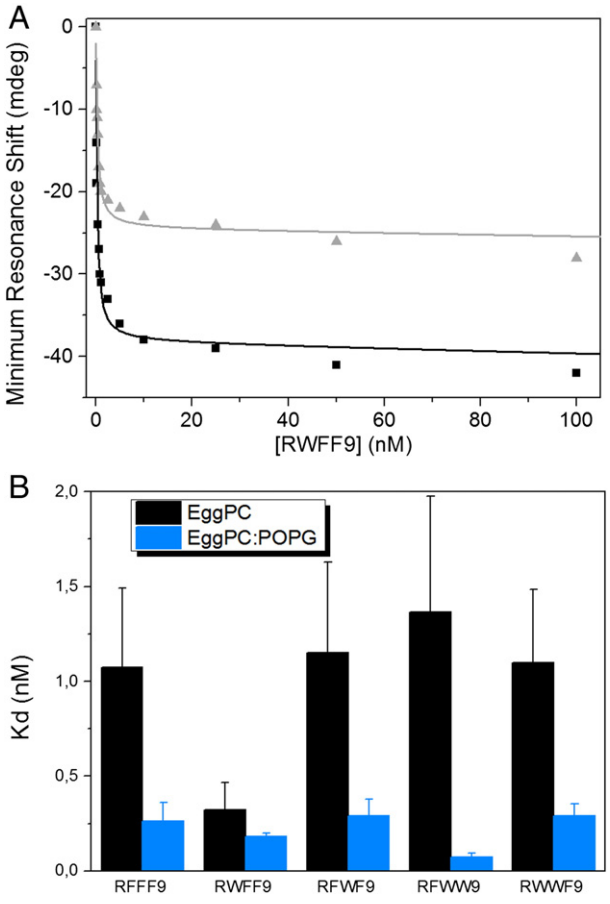

Fig. 4. Interaction of the peptides with the bilayer monitored by PWR. (A) Shifts in the resonance minimum upon interaction of increasing concentrations of peptide with the bilayer for *p*- and *s*-polarization (black curve and gray curve respectively). (B) Dissociation constants (K_D) determined with PWR for peptide interaction with EggPC (black bars) and EggPC:POPG (4:1 mol:mol) (blue bars) supported bilayers. The experiments were done in triplicate at room temperature.

that a decrease in the mass of the system occurs upon peptide addition (Fig. 4). This might be due to a detergent effect of the peptide leading to partial removal of lipid from the membrane or to a reorganization of the lipids induced by the peptide leading to an overall higher surface area occupied by each lipid.

By following the resonance position shifts upon incremented addition of peptide and fitting with a hyperbolic function, K_D values were obtained (see Materiel & methods for details). An affinity in the nanomolar range was observed for all peptide interactions and both membrane compositions; however the affinity was slightly higher in the case of anionic lipids (K_D ~ 1 nM for zwitterionic lipids and ~0.2 nM for anionic lipids; Fig. 4B). This agrees well with the results obtained by fluorescence studies (K_{SV} and "half-binding" constants) presented previously, indicating enhanced interaction and insertion with anionic lipids. After reaching peptide saturation (plateau), the lipid membrane was washed by flowing buffer through the cell in order to test whether peptide binding and effect on membranes were reversible. We observe a correlation between the number of Trp residues and the reversibility of the interaction, the lower the number of Trp residues, the less reversible being the interaction (Fig. 5). We interpret this observation as follows: Phe residues being more hydrophobic than Trp allows the peptide to be more deeply inserted in the membrane and therefore in a less reversible and a more permanent manner. Washing the membrane in the case of RW9 leads to an almost complete recovery of the membrane signal obtained before peptide addition (almost completely reversible binding). The data allow us to conclude that the aromaticity of the amino-acids is important for the peptide membrane translocation but a high hydrophobicity of such residues prevents the peptide translocation due to a deeper and/or more irreversible lipid interaction.

3.6. Peptide insertion in the membrane

The studies of tryptophan fluorescence quenching by brominated lipids provide information about the membrane insertion level of the peptides. The Trp insertion depth from the bilayer center for the RX9 analogs was obtained for DOPC/DOPG (4:1) LUVs. The average Trp insertion level of the RX9 and RW9 is around 10–11 Å from the membrane center, according to both Distribution Analysis (DA) and Parallax Method (PM) analysis (Table 5; Fig. S3), thus Trp residues are located just below the lipid polar headgroups. Overall the peptides with 2 Phe residues are slightly more inserted in the bilayer (~9 Å) than the one with 1 Phe (~11 Å). This is consistent with the reversibility of the binding of the peptides observed with PWR.

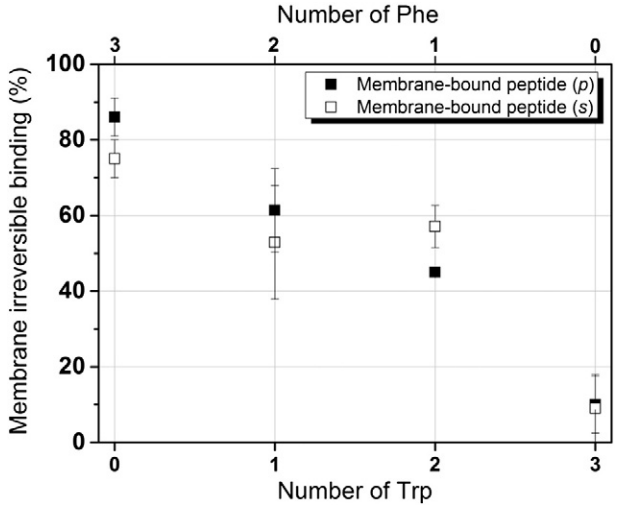

Fig. 5. Percentage of "washing-resistant" or irreversible membrane-bound peptide after a washing step of the PWR cell (2 mL) represented as a function of the number of Trp and Phe residues.

Table 5
Average insertion depth of the peptides in DOPC:DOPG (4:1) LUVs determined by the Distribution Analysis (DA) and Parallax Methods (PM) together with the respective method fitting parameters. The experiments have been done on in triplicate at room temperature.

	DA			PM	
	h_m (Å)	σ (Å)	S	h_m (Å)	R_c (Å)
RW_9	10.4 ± 0.9	5.8 ± 1.2	1.3 ± 0.5	10.2 ± 0.7	8.2 ± 1.4
$RWFF_9$	9.7 ± 0.5	2.6 ± 0.4	0.6 ± 0.1	9.9 ± 0.8	4.8 ± 1.2
$RFWF_9$	9.9 ± 0.2	2.3 ± 0.4	0.3 ± 0.1	10.6 ± 0.9	5.1 ± 0.4
$RFWW_9$	11.2 ± 1	2.9 ± 1	0.7 ± 0.5	12.7 ± 0.1	7 ± 1
$RWWF_9$	11 ± 0.8	3.8 ± 1.2	0.9 ± 0.6	11.1 ± 0.5	6.5 ± 1.3

The study shows that the higher hydrophobicity of the Phe plays an important role in peptide insertion and depth in anionic membranes. If one assumes that the peptides are mostly structured in helical conformation their backbone should be located around 16 Å from the bilayer center. Molecular dynamic simulation (MDS) data obtained on RW9 show an insertion depth of the peptide backbone of 14 Å from the bilayer center. The results are thus comparable, the small difference observed can arise from the time range differences between the two experiments that are much longer in these studies than in MDS. We could not obtain results with DOPC liposomes with the brominated lipid quenching experiments. This could be due to the fact that with DOPC the peptides interact more superficially and with slightly smaller affinity than with anionic liposomes.

The peptide effect on the membrane lipid orientation and organization was examined by polarized ATR-FTIR experiments (Table 6). Such experiments allow one to calculate the dichroic ratio ($R_{ATR} = Ap/As$) relative to the symmetric CH_2 vibration mode (ν_s CH_2) of the lipid chains (around 2853 cm^{-1}) and how that was affected by the peptides. Such ratio provides information about the peptide effect on the lipid chain ordering and orientation. We have observed a slight increase in the R_{ATR} of DOPC lipids in presence of most of the RX9 peptides (except RWFF9) corresponding to a slight disorganization of the lipid chains. On the contrary a slight decrease of the R_{ATR} was observed with anionic membranes (DOPC:DOPG 4:1) indicating that the peptide further organized these lipids. This probably results from the fact that peptide interaction with anionic lipids leads to a decrease of the repulsive forces between the lipid headgroups and thus an increase in ordering and packing of the membrane. This correlates well with calcein leakage experiments in which no leakage was observed with anionic lipids and a slight leakage was observed with zwitterionic lipids. However no significant differences were evidenced among the RX9 peptides leading us to conclude that membrane perturbation induced by the peptides is not a property that could explain the observed differences in cellular internalization.

4. Conclusion

Herein we have investigated the role of Trp residues in the cellular internalization and membrane interaction properties of the RW9 CPP. While arginine role has been thoroughly investigated and established

Table 6
Dichroïc ratio (R_{ATR}) of symmetric carbonyl lipid stretching (ν_s CH_2) around 2853 cm^{-1} for DOPC and DOPC:DOPG (4:1) in the absence and in the presence of 5 nmol of RX9 peptides.

Peptides	DOPC	+ peptide	DOPC:DOPG	+ peptide
RFFF9	1.45 ± 0.1	1.62 ± 0.08	1.4 ± 0.09	1.42 ± 0.03
RWFF9	1.53 ± 0.1	1.47 ± 0.1	1.5 ± 0.06	1.35 ± 0.1
RFWF9	1.44 ± 0.1	1.5 ± 0.1	1.41 ± 0.05	1.33 ± 0.05
RFWW9	1.39 ± 0.07	1.46 ± 0.01	1.39 ± 0.07	1.38 ± 0.05
RWWF9	1.28 ± 0.09	1.4 ± 0.1	1.4 ± 0.04	1.37 ± 0.09

[50,51] that of aromatic residues has received far less attention. For RW9, the substitution of Trp by Leu residues has been reported to remove the cell penetrating ability of the peptide pointing to the importance of Trp residues [19]. On the contrary, R9 is known as a performing CPP from previous studies [7,19], leaving open questions on the role of aromatic residues. The substitution of Trp by Phe residues in the RW9 sequence leads to a major decrease in the cellular internalization, which was almost abolished for the peptide containing no Trp residues. In contrast, their membrane accumulation was retained.

Different modes of CPP internalization, direct translocation and endocytosis, can occur. Direct translocation implies that the peptides directly reach the cytosol of cells. In contrast, a peptide that enters through endocytosis, a process that is inhibited at temperatures below 12 °C, ends up into endosomes from which it has to escape to reach the cytosol of cells. For drug delivery purposes, only the fraction of the peptide that is not entrapped in endosomes is relevant.

RW9 has been shown previously to enter cells by both direct translocation of the plasma membrane and endocytosis [19]. By comparing RW9 cellular uptake at 4 and 37 °C in wild-type (wt) and GAG-deficient CHO cells, it was found that 85% of the CPP internalized in wt cells at 37 °C entered by GAG-dependent endocytosis and 15% by direct translocation. We observed here that internalization of all the RX9 peptides at 37 °C is extremely low and is in almost all cases decreased more than 10 times compared to RW9. This suggests that both endocytosis and direct translocation are affected by the replacement of Trp residues with Phe residues. However, we could not perform internalization experiments at 4 °C with the RX9 peptides to measure their entry exclusively by direct translocation because as shown, the amounts of internalized peptide were already quite low at 37 °C. At 4 °C due to endocytosis blockage, one expects the internalization to be even lower, as observed for RW9 peptide [19], and therefore impossible to measure for the RX9 peptides.

The role of Trp residues in the recruitment of cell-surface GAGs to trigger endocytosis has been investigated before using biophysical methods [12,52]. In contrast, the implication of this amino acid in direct translocation is still not fully understood, although Rydberg et al. have recently highlighted that tryptophan position in dodecapeptide Arg/Trp sequences affects cytotoxicity and the way these peptides interact with the different model membranes [53,54].

We performed here a complete biophysical study of RW9 and RX9 analogs aimed at correlating their cellular uptake properties to better understand the role of Trp residues in direct translocation of the plasma membrane. We showed that in the presence of lipids their secondary structure was not modified even if they are mostly unstructured. Contrarily to what the literature suggests for some CPPs [55], the cellular internalization of these peptides is not directly correlated to their secondary structure.

Despite the fact that all peptides accumulate and partition in the membrane in the same way, we concluded that their anchoring in the membrane is directly dependent on the hydrophobicity and interfacial properties of the amino-acids. Arg residues drive their binding to the membrane and are responsible for their membrane accumulation and partition, explaining their enhanced interaction with anionic lipids. Following such interaction, Arg residues play the role of hinge allowing insertion of the hydrophobic residues more deeply into the membrane. At this point the nature of the hydrophobic residues is detrimental to the CPP fate in terms of the reversibility of the membrane interaction and ultimate membrane crossing. Indeed our studies reveal that less hydrophobic residues and more interfacial ones will help the peptides to establish more transitory interactions with the membrane in part due to a less deep membrane insertion. Such malleable membrane interaction and peptide structural change are important to avoid the peptide from being retained in the membrane interior and to trigger translocation into membranes. This study demonstrates that not only the number but also the nature and the positioning of the hydrophobic residues, their aromaticity and interfacial properties are important for their membrane translocation. Penetrating properties are favored when Trp residues form a large hydrophobic peptide face. Additionally, Trp residues in positions 4 and 7 of the RW9 sequence have been shown to promote π–cation interactions important to partially mask the peptide charge and decrease the energy barrier for membrane translocation [19]. Overall, membrane interaction should allow peptide accumulation but a deep membrane insertion should be avoided in order to favor more transitory interactions and allow membrane translocation.

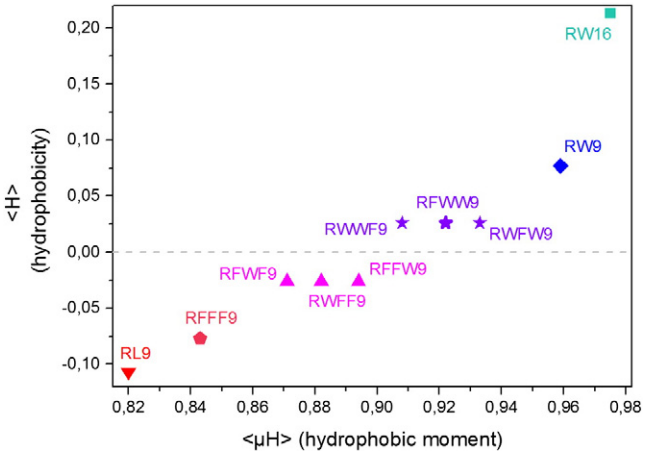

Fig. 6. Hydrophobic plot of RW9, RL9, RW16 and RX9 analogues. The abscissa gives the helical hydrophobic moment (<μH>) of each peptide and the ordinate gives the corresponding values of hydrophobicity (<H>). The peptide that is most internalized is represented in blue with a gradient to the red for the peptides which are the less internalized. RW16 is represented in light blue and is well internalized with increasing cytotoxicity.

To reinforce this idea, we have calculated the hydrophobic moment for all RW9 and RX9 peptides, the helical projections of the peptides were performed (Fig. S5) and a plot representing hydrophobicity vs. hydrophobic moment of the peptides allowed us to visualize the differences in terms of hydrophobicity between each peptide (Fig. 6). Hydrophobic plot indicated that diminution of hydrophobicity and amphipathicity of the RX9 peptides decreases its cellular uptake and that the substantial increase of these parameters leads to an increase of their cytotoxicity. This suggests that a fine tuning of these parameters exists to enhance CPP internalization and that above this threshold value toxicity starts to develop.

Acknowledgments

This work was funded by the French Ministère de l'Enseignement Supérieur et de la Recherche. We thank Cathy Staedel (Inserm U869, Univ-Bordeaux) for providing CHO-K1 cells and Alexandra Milochau and Julien Gaitan (CNRS UMR5248 CBMN Univ-Bordeaux) for the assistance in cell culture for cytotoxicity tests. We thank Gérard Bolbach (CNRS UMR7203 LBM UPMC Univ-Paris6) for assistance in the use of the MALDI-TOF mass spectrometry. We thank Manuel N. Melo for his help with the fitting of the three-state model in Trp fluorescence.

Appendix A. Supplementary data

Supplementary data to this article can be found online at http://dx.doi.org/10.1016/j.bbamem.2014.11.013.

References

[1] G.P. Dietz, M. Bahr, Delivery of bioactive molecules into the cell: the Trojan horse approach, Mol. Cell. Neurosci. 27 (2004) 85–131.
[2] A.D. Frankel, C.O. Pabo, Cellular uptake of the tat protein from human immunodeficiency virus, Cell 55 (1988) 1189–1193.
[3] M. Green, P.M. Loewenstein, Autonomous functional domains of chemically synthesized human immunodeficiency virus tat trans-activator protein, Cell 55 (1988) 1179–1188.

[4] E. Vives, P. Brodin, B. Lebleu, A truncated HIV-1 Tat protein basic domain rapidly translocates through the plasma membrane and accumulates in the cell nucleus, J. Biol. Chem. 272 (1997) 16010–16017.
[5] D. Derossi, A.H. Joliot, G. Chassaing, A. Prochiantz, The third helix of the *Antennapedia* homeodomain translocates through biological membranes, J. Biol. Chem. 269 (1994) 10444–10450.
[6] P.A. Wender, D.J. Mitchell, K. Pattabiraman, E.T. Pelkey, L. Steinman, J.B. Rothbard, The design, synthesis, and evaluation of molecules that enable or enhance cellular uptake: peptoid molecular transporters, Proc. Natl. Acad. Sci. U. S. A. 97 (2000) 13003–13008.
[7] S. Futaki, T. Suzuki, W. Ohashi, T. Yagami, S. Tanaka, K. Ueda, Y. Sugiura, Arginine-rich peptides. An abundant source of membrane-permeable peptides having potential as carriers for intracellular protein delivery, J. Biol. Chem. 276 (2001) 5836–5840.
[8] D. Derossi, S. Calvet, A. Trembleau, A. Brunissen, G. Chassaing, A. Prochiantz, Cell internalization of the third helix of the *Antennapedia* homeodomain is receptor-independent, J. Biol. Chem. 271 (1996) 18188–18193.
[9] F. Duchardt, M. Fotin-Mleczek, H. Schwarz, R. Fischer, R. Brock, A comprehensive model for the cellular uptake of cationic cell-penetrating peptides, Traffic 8 (2007) 848–866.
[10] S. El Andaloussi, P. Guterstam, U. Langel, Assessing the delivery efficacy and internalization route of cell-penetrating peptides, Nat. Protoc. 2 (2007) 2043–2047.
[11] P. Guterstam, F. Madani, H. Hirose, T. Takeuchi, S. Futaki, S. El Andaloussi, A. Graslund, U. Langel, Elucidating cell-penetrating peptide mechanisms of action for membrane interaction, cellular uptake, and translocation utilizing the hydrophobic counter-anion pyrenebutyrate, Biochim. Biophys. Acta 1788 (2009) 2509–2517.
[12] C.Y. Jiao, D. Delaroche, F. Burlina, I.D. Alves, G. Chassaing, S. Sagan, Translocation and endocytosis for cell-penetrating peptide internalization, J. Biol. Chem. 284 (2009) 33957–33965.
[13] A. Mishra, V.D. Gordon, L. Yang, R. Coridan, G.C. Wong, HIV TAT forms pores in membranes by inducing saddle-splay curvature: potential role of bidentate hydrogen bonding, Angew. Chem. Int. Ed. Engl. 47 (2008) 2986–2989.
[14] J.B. Rothbard, T.C. Jessop, P.A. Wender, Adaptive translocation: the role of hydrogen bonding and membrane potential in the uptake of guanidinium-rich transporters into cells, Adv. Drug Deliv. Rev. 57 (2005) 495–504.
[15] A. Ziegler, J. Seelig, Binding and clustering of glycosaminoglycans: a common property of mono- and multivalent cell-penetrating compounds, Biophys. J. 94 (2008) 2142–2149.
[16] A. Ziegler, J. Seelig, Contributions of glycosaminoglycan binding and clustering to the biological uptake of the nonamphipathic cell-penetrating peptide WR9, Biochemistry 50 (2011) 4650–4664.
[17] B. Christiaens, S. Symoens, S. Verheyden, Y. Engelborghs, A. Joliot, A. Prochiantz, J. Vandekerckhove, M. Rosseneu, B. Vanloo, Tryptophan fluorescence study of the interaction of penetratin peptides with model membranes, Eur. J. Biochem. 269 (2002) 2918–2926.
[18] D. Delaroche, B. Aussedat, S. Aubry, G. Chassaing, F. Burlina, G. Clodic, G. Bolbach, S. Lavielle, S. Sagan, Tracking a new cell-penetrating (W/R) nonapeptide, through an enzyme-stable mass spectrometry reporter tag, Anal. Chem. 79 (2007) 1932–1938.
[19] A. Walrant, I. Correia, C.Y. Jiao, O. Lequin, E.H. Bent, N. Goasdoue, C. Lacombe, G. Chassaing, S. Sagan, I.D. Alves, Different membrane behaviour and cellular uptake of three basic arginine-rich peptides, Biochim. Biophys. Acta 1808 (2011) 382–393.
[20] D. Derossi, G. Chassaing, A. Prochiantz, Trojan peptides: the penetratin system for intracellular delivery, Trends Cell Biol. 8 (1998) 84–87.
[21] I.D. Alves, Membrane-active peptides: mechanisms of action, Curr. Protein Pept. Sci. 13 (2012) 601.
[22] P. Joanne, C. Galanth, N. Goasdoue, P. Nicolas, S. Sagan, S. Lavielle, G. Chassaing, C. El Amri, I.D. Alves, Lipid reorganization induced by membrane-active peptides probed using differential scanning calorimetry, Biochim. Biophys. Acta 1788 (2009) 1772–1781.
[23] J. Connor, C. Bucana, I.J. Fidler, A.J. Schroit, Differentiation-dependent expression of phosphatidylserine in mammalian plasma membranes: quantitative assessment of outer-leaflet lipid by prothrombinase complex formation, Proc. Natl. Acad. Sci. U. S. A. 86 (1989) 3184–3188.
[24] B. Frey, U.S. Gaipl, The immune functions of phosphatidylserine in membranes of dying cells and microvesicles, Semin. Immunopathol. 33 (2011) 497–516.
[25] S. Ran, A. Downes, P.E. Thorpe, Increased exposure of anionic phospholipids on the surface of tumor blood vessels, Cancer Res. 62 (2002) 6132–6140.
[26] T. Utsugi, A.J. Schroit, J. Connor, C.D. Bucana, I.J. Fidler, Elevated expression of phosphatidylserine in the outer membrane leaflet of human tumor cells and recognition by activated human blood monocytes, Cancer Res. 51 (1991) 3062–3066.
[27] V.V. Andrushchenko, H.J. Vogel, E.J. Prenner, Optimization of the hydrochloric acid concentration used for trifluoroacetate removal from synthetic peptides, J. Pept. Sci. 13 (2007) 37–43.
[28] F. Burlina, S. Sagan, G. Bolbach, G. Chassaing, A direct approach to quantification of the cellular uptake of cell-penetrating peptides using MALDI-TOF mass spectrometry, Nat. Protoc. 1 (2006) 200–205.
[29] E. Goormaghtigh, V. Cabiaux, J.M. Ruysschaert, Secondary structure and dosage of soluble and membrane proteins by attenuated total reflection Fourier-transform infrared spectroscopy on hydrated films, Eur. J. Biochem. 193 (1990) 409–420.
[30] E. Goormaghtigh, V. Raussens, J.M. Ruysschaert, Attenuated total reflection infrared spectroscopy of proteins and lipids in biological membranes, Biochim. Biophys. Acta 1422 (1999) 105–185.
[31] M.L. Jobin, P. Bonnafous, H. Temsamani, F. Dole, A. Grelard, E.J. Dufourc, I.D. Alves, The enhanced membrane interaction and perturbation of a cell penetrating peptide in the presence of anionic lipids: toward an understanding of its selectivity for cancer cells, Biochim. Biophys. Acta 1828 (2013) 1457–1470.
[32] M.N. Melo, M.A. Castanho, Omiganan interaction with bacterial membranes and cell wall models. Assigning a biological role to saturation, Biochim. Biophys. Acta 1768 (2007) 1277–1290.
[33] A.S. Ladokhin, Distribution analysis of depth-dependent fluorescence quenching in membranes: a practical guide, Methods Enzymol. 278 (1997) 462–473.
[34] A.S. Ladokhin, P.W. Holloway, E.G. Kostrzhevska, Distribution analysis of membrane penetration of proteins by depth-dependent fluorescence quenching, J. Fluoresc. 3 (1993) 195–197.
[35] F.S. Abrams, E. London, Calibration of the parallax fluorescence quenching method for determination of membrane penetration depth: refinement and comparison of quenching by spin-labeled and brominated lipids, Biochemistry 31 (1992) 5312–5322.
[36] F.S. Abrams, E. London, Extension of the parallax analysis of membrane penetration depth to the polar region of model membranes: use of fluorescence quenching by a spin-label attached to the phospholipid polar headgroup, Biochemistry 32 (1993) 10826–10831.
[37] A. Chattopadhyay, E. London, Parallax method for direct measurement of membrane penetration depth utilizing fluorescence quenching by spin-labeled phospholipids, Biochemistry 26 (1987) 39–45.
[38] P.E. Thoren, D. Persson, E.K. Esbjorner, M. Goksor, P. Lincoln, B. Norden, Membrane binding and translocation of cell-penetrating peptides, Biochemistry 43 (2004) 3471–3489.
[39] I.D. Alves, S.M. Cowell, Z. Salamon, S. Devanathan, G. Tollin, V.J. Hruby, Different structural states of the proteolipid membrane are produced by ligand binding to the human delta-opioid receptor as shown by plasmon-waveguide resonance spectroscopy, Mol. Pharmacol. 65 (2004) 1248–1257.
[40] Z. Salamon, G. Tollin, Optical anisotropy in lipid bilayer membranes: coupled plasmon-waveguide resonance measurements of molecular orientation, polarizability, and shape, Biophys. J. 80 (2001) 1557–1567.
[41] Z. Salamon, G. Tollin, I. Alves, V. Hruby, Chapter 6. Plasmon resonance methods in membrane protein biology applications to GPCR signaling, Methods Enzymol. 461 (2009) 123–146.
[42] G. Drin, S. Cottin, E. Blanc, A.R. Rees, J. Temsamani, Studies on the internalization mechanism of cationic cell-penetrating peptides, J. Biol. Chem. 278 (2003) 31192–31201.
[43] H.L. Lee, E.A. Dubikovskaya, H. Hwang, A.N. Semyonov, H. Wang, L.R. Jones, R.J. Twieg, W.E. Moerner, P.A. Wender, Single-molecule motions of oligoarginine transporter conjugates on the plasma membrane of Chinese hamster ovary cells, J. Am. Chem. Soc. 130 (2008) 9364–9370.
[44] B. Christiaens, J. Grooten, M. Reusens, A. Joliot, M. Goethals, J. Vandekerckhove, A. Prochiantz, M. Rosseneu, Membrane interaction and cellular internalization of penetratin peptides, Eur. J. Biochem. 271 (2004) 1187–1197.
[45] S.T. Henriques, M.A. Castanho, Environmental factors that enhance the action of the cell penetrating peptide pep-1 A spectroscopic study using lipidic vesicles, Biochim. Biophys. Acta 1669 (2005) 75–86.
[46] N.C. Santos, M. Prieto, M.A. Castanho, Quantifying molecular partition into model systems of biomembranes: an emphasis on optical spectroscopic methods, Biochim. Biophys. Acta 1612 (2003) 123–135.
[47] P.M. Matos, H.G. Franquelim, M.A. Castanho, N.C. Santos, Quantitative assessment of peptide–lipid interactions. Ubiquitous fluorescence methodologies, Biochim. Biophys. Acta 1798 (2010) 1999–2012.
[48] M. Rodrigues, A. Santos, B.G. de la Torre, G. Radis-Baptista, D. Andreu, N.C. Santos, Molecular characterization of the interaction of crotamine-derived nucleolar targeting peptides with lipid membranes, Biochim. Biophys. Acta 1818 (2012) 2707–2717.
[49] A. Walrant, A. Vogel, I. Correia, O. Lequin, B.E. Olausson, B. Desbat, S. Sagan, I.D. Alves, Membrane interactions of two arginine-rich peptides with different cell internalization capacities, Biochim. Biophys. Acta 1818 (2012) 1755–1763.
[50] C. Bechara, S. Sagan, Cell-penetrating peptides: 20 years later, where do we stand? FEBS Lett. 587 (2013) 1693–1702.
[51] M. Nishihara, F. Perret, T. Takeuchi, S. Futaki, A.N. Lazar, A.W. Coleman, N. Sakai, S. Matile, Arginine magic with new counterions up the sleeve, Org. Biomol. Chem. 3 (2005) 1659–1669.
[52] C. Bechara, M. Pallerla, Y. Zaltsman, F. Burlina, I.D. Alves, O. Lequin, S. Sagan, Tryptophan within basic peptide sequences triggers glycosaminoglycan-dependent endocytosis, FASEB J. 27 (2013) 738–749.
[53] H.A. Rydberg, A. Kunze, N. Carlsson, N. Altgarde, S. Svedhem, B. Norden, Peptide-membrane interactions of arginine-tryptophan peptides probed using quartz crystal microbalance with dissipation monitoring, Eur. Biophys. J. 43 (2014) 12.
[54] H.A. Rydberg, M. Matson, H.L. Amand, E.K. Esbjorner, B. Norden, Effects of tryptophan content and backbone spacing on the uptake efficiency of cell-penetrating peptides, Biochemistry 51 (2012) 5531–5539.
[55] S. Deshayes, T. Plenat, G. Aldrian-Herrada, G. Divita, C. Le Grimellec, F. Heitz, Primary amphipathic cell-penetrating peptides: structural requirements and interactions with model membranes, Biochemistry 43 (2004) 7698–7706.